Delft University of Technology

Urban Air Mobility

TU Delft Online Learning

eVTOL Structural Analysis & Optimisation

2023

Nomenclature

Table 1: Nomenclature

Symbol	Name	Unit
λ	Taper Ratio	–
a/b	Wing-box Aspect Ratio	m
b	Total wing span	m
b_{st}	Stringer Pitch	m
b_i	Base Shear Flow	N/m
h	Half of Wing-box Height	m
h_{st}	Stringer Height	m
w_{st}	Stringer Flange Width	m
c	Chord	m
k	Buckling Coefficient	-
n	Load Factor	-
t	Thickness	m
x	Chord-wise (x) coordinate	m
y	Span-wise (y) coordinate	m
z	Thickness-wise (z) coordinate	m
q	Shear Flow	N/m
l	Trailing Edge Skin Length	m
L	Rib Pitch	m
A	Area	m^2
E	E-modulus	GPa
F or P	Force	N
H	Wing-box Height	m
N	Distributed Force	N/m
I	Moment of Inertia	m^4
V	Shear Force	N
W	Weight	N
σ	Stress	MPa
τ	Shear Stress	MPa
ρ	Density	kg/m^2
ν	Poisson ratio	-
β, m, g	Crippling Material Constants	-

Table 2: Subscripts

Subscript	Name
LE	Leading edge
TE	Trailing edge
sp	Spar
sk	Skin
st	Stringer
r	Root

1 Introduction

The structure that carries most of the aerodynamic load is the wing-box. Given an aerodynamic loading due to the wing planform and airfoil shape, there are multiple solutions for the internal architecture of the wing box that could meet the strength and stiffness requirements. However, one solution can lead to a lower wing weight compared to other structural layouts. Hence, a local structural optimisation of the internal architecture of the wing is performed after a global optimisation of the wing planform for aerodynamic, performance, control and stability considerations.

Preliminary design is always performed with the use of analytical equations, due to the fast and simple approach for accurate initial values. Once a preliminary design is achieved, FEM solutions provide more reliable structural assessment. It is also worth mentioning that once the analysis tools are created, the optimization can take take place by trial and error. An optimiser should be wisely used, with sensible choice of initial values and boundaries. Note that if the initial design fed to the optimiser is not feasible and realistic, the optimisation will not work!

The modeled wing is rectangular, with a taper ratio equal to 0.45, 0 sweep and airfoil NACA 44017, sized for aerodynamic loading only and for a maximum take off mass of 2124 kg (given the fact that the eVTOL has two wings, one wing is sized for 1062 kg), with three engines mounted on each half, symmetrically [1]. In the current optimisation framework, a metallic wing will be assessed, with no structural instability (buckling) or yielding allowed in cruise condition, when the loading factor (lift divided by weight) is 1, and failure is not allowed for a load factor below 2.5. It is common engineering practice to add safety factors to the loads, usually between 1.1 and 1.5, however, for this exercise purpose, the used safety factor is 1, as the limits of the light-weight design are tested. Due to symmetry, only half of a wing is analysed.

2 Wing Modelling and Optimisation Set-up

In order to ease the calculations, the structure is idealised, various assumptions being performed. Throughout the structural analysis, the following assumptions are considered:

- Symmetric cross-section
- Thin-walled assumption
- Stringers carry the bending loads
- Only the skin and spar webs carry the shear load
- The wing is modelled as a clamped beam at the root using the Euler–Bernoulli beam theory, thus assuming only small deflections occur in the wing. For large wing deflections, the theory does not hold anymore
- The wing is sized for lift only (preliminary design), given the drag is significantly smaller [1].

The cross-section of the wing box is considered to be symmetric, a rectangle, and its geometry begins at the location of the leading edge spar, located at 15% of the chord, and ends at the location of the trailing edge spar, located at 75% of the chord. The location of the two spars is typical, as it allows for effective use of high-lift devices, and the spars are modelled as I-beams. For the NACA 44017 airfoil, the maximum chord to height ratio is 0.17, Equation 1 and Equation 2 being utilised to define the local chord length and wing-box height as a function of the span-wise location.

$$c(y) = c_r - c_r(1-\lambda)\frac{y}{b/2} \quad (1) \qquad H(y) = 0.17 \cdot c(y) \quad (2)$$

Throughout the design optimisation Z-shaped stringers have been assumed, which is a typical profile utilised for the stringers. The stringers are parameterised in the optimisation through the width of the two flanges, the height of the web and the stringer thickness, considered constant. The area and moment of inertia of one stringer are then simply defined in Equation 3 and Equation 4. The moment of inertia is computed by applying the formula for rectangles and Steiner terms, and the second term in Equation 4 can be neglected due to thin wall assumptions.

$$A_{st} = t_{st} \cdot (2 \cdot w_{st} + h_{st}) \quad (3) \qquad I_{st} = \frac{t_{st} h_{st}^3}{12} + \frac{w_{st} t_{st}^3}{12} + 2A_{st}\left(\frac{h_{st}}{2}\right)^2 \quad (4)$$

The ribs are modelled as rectangles as well, with the length equal to 0.6 of the local chord length as given by Equation 1, and the height as given by Equation 2. They also define stations at which loads are calculated and they delimit different skin panels.

Based on the wing box parametrisation, the design vector is given by Equation 5, continuous variables being utilised. With the exception of t, which is a vector, all the other variables are scalars.

$$X = [b, c_r, t_{sp}, t_{rib}, L, b_{st}, h_{st}, t_{st}, w_{st}, t] \quad (5)$$

The leading and trailing edges contribute towards the wing weight and shear carrying capabilities, hence they have to be modelled as well. The leading edge has been modelled as a semi-ellipse (but could have been modelled as a semi-circle as well), thus the perimeter of the leading edge is given in Equation 6. The trailing edge is modelled as a triangle, and the length of one edge is given in Equation 7.

$$LE(y) = \pi \cdot \left(3 \cdot (0.5 \cdot h(z) + 0.15 \cdot c(y)) - \sqrt{(3 \cdot 0.5 \cdot h(y) + 0.15 \cdot c(y)) \cdot (0.5 \cdot h(y) + 3 \cdot 0.15 \cdot c(y))}\right) \quad (6)$$

$$l_{sk}(y) = \sqrt{h(y)^2 + (0.25c(y))^2} \quad (7)$$

Given the wing box parametrisation and the leading and trailing edge modelling as a function of the variables, the weight of one panel is computed as an integral with respect to the panel length, as in Equation 8.

$$W_{panel} = \int_{y1}^{y2} \rho \cdot (2 \cdot c(y) \cdot t_{skin} + 2 \cdot h(y) \cdot t_{spar} + 2 \cdot l_{sk}(y) \cdot t_{sk} + 2 \cdot n_{st} \cdot A_{st}(y) + LE(y))dy \quad (8)$$

The weight of one rib is computed in Equation 9.

$$W_{rib} = \rho \cdot 0.6c(z) \cdot h(z) \cdot t_{rib} \quad (9)$$

The objective function, represented by (half of) the wing weight, is given in Equation 10, and is the result of all panels and ribs weight summation.

$$W_{wing} = \sum W_{panel} + \sum W_{rib} \quad (10)$$

For the shear force computation due to weight distribution, the weights of the ribs and the engines are considered to be point loads. In the code implementation, the weight of a panel as resulted from Equation 8 is assigned at its root rib. As the weight of each panel and each rib is known, a linear interpolation is performed between the stations, defined by the ribs. A demonstrative shear diagram due to weight distribution is depicted in Figure 1, with absolute values (lift and weight have opposite signs, but for ease, the magnitude of the forces is depicted; though, for correctness and consistency with the coordinate system, the values should be negative).

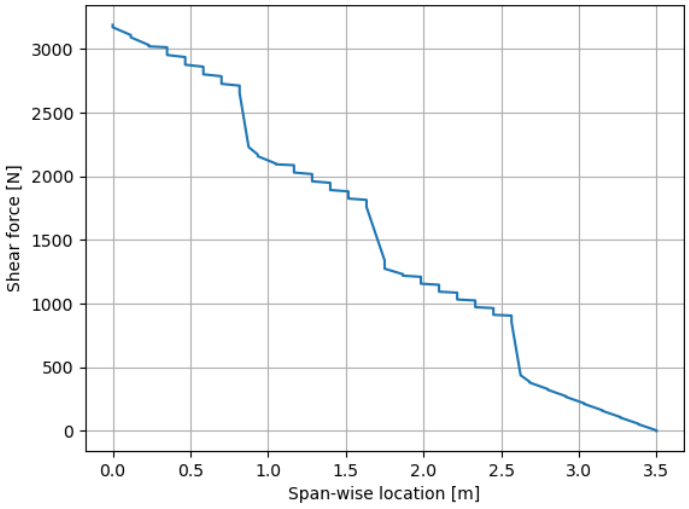

Figure 1: Shear Distribution due to Weight

3 Shear Flow Calculations

The span-wise aerodynamic loading function can be obtained with **??** as a quadratic interpolation of the local lift coefficients computed with W theory, scaled by the dynamic pressure, assumed constant for cruising conditions. However, note that due to the span-wise discretisation, the function can not be coupled with the structural optimiser, as the resulting function used in constraint definitions is not differentiable. Hence, the span-wise lift should be computed for a certain span and root chord.

$$L(y) = ccl(y) \cdot q \tag{11}$$

Since the tutorial is on structural analysis, the aerodynamic loading can also be considered linearly distributed. As the eVTOL has two wings, one half of the wing must be able to carry a quarter of the weight. As previously stated, the maximum take-off mass is 2124 kg. The corresponding aerodynamic load distribution is given by Equation 12.

$$aero\ load(y) = (-151.7143y + 531) \cdot 9.81 \tag{12}$$

Given a final shear loading resulted from the superposition between the aerodynamic load and weight, a shear flow is generated and can be computed at any location through the cross-section. The final shear force distribution is depicted in Figure 2.

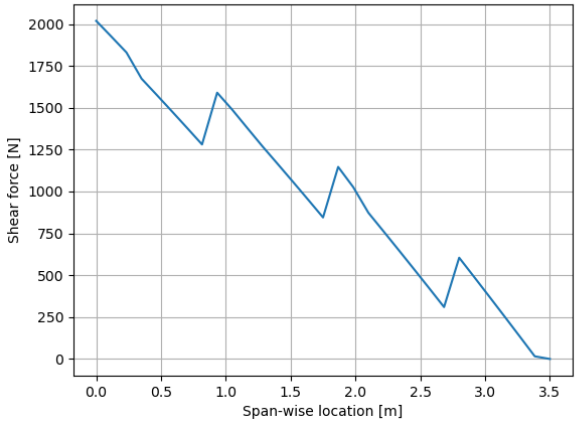

Figure 2: Final Shear Force Diagram

The total shear flow at a certain point is the result of the superposition between the base and the redundant shear flow. Figure 3 depicts the airfoil idealisation and the shear flow components.

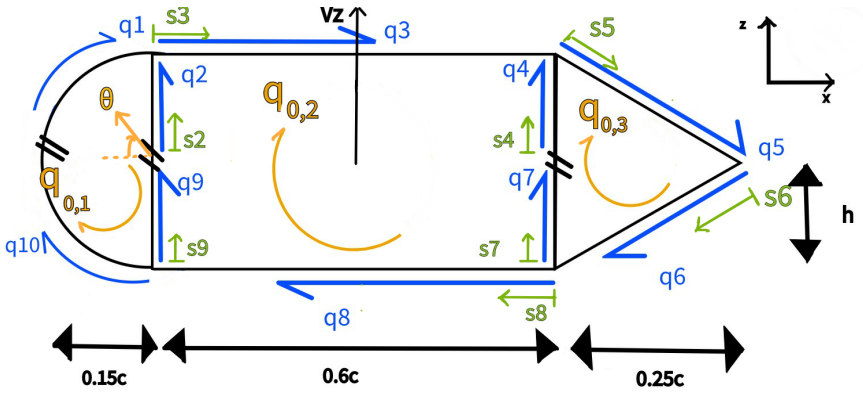

Figure 3: Cross section view for shear flow

The general formula to compute the base shear flow at a certain location in the cross section with constant thickness as a function of the geometry is given in Equation 13, where z is the z-coordinate of the point and ds is the increment along the perimeter [4]. In the current analysis V_x is 0.

$$q(s) = \int_0^s \frac{\delta q}{\delta s} ds = -\frac{V_z t}{I_{xx}} \int_0^s z ds - \frac{V_x t}{I_{zz}} \int_0^s x ds = -\frac{V_z t}{I_{xx}} \int_0^s z ds \tag{13}$$

Region 1

Because of the curved nature of the geometry, polar coordinates are more convenient to use. Using small angle approximation where $\sin \cdot d\theta = d\theta$, ds_1 can be substituted with $hd\theta$ (ds_1=$hd\theta$) and the z coordinate is equal to $h \cdot sin\theta$.

$$q_{b_1}(\theta) = -\frac{V_z t_{sk}}{I_{xx}} \int_0^\theta h^2 sin\theta \cdot d\theta = \frac{V_z t_{sk}}{I_{xx}} h^2 (cos\theta - 1), \quad 0 \leq \theta \leq \pi/2 \tag{14}$$

Region 2

Given the vertical orientation of the spar web, the integration in region 2 can be performed as a function of z, with $ds_2 = dz$.

$$q_{b_2}(z) = -\frac{V_z t_{sp}}{I_{xx}} \int_0^z z \cdot dz = -\frac{V_z t_{sp}}{2I_{xx}} z^2, \quad 0 \leq z \leq h \tag{15}$$

Region 3

In region 3, the z coordinate is constant and equal to half of the total height of the spar web.

$$q_{b3}(s_3) = -\frac{V_z t_{sk}}{I_{xx}} \int_0^{s3} h \cdot ds_3 + q_{b_1}(\pi/2) + q_{b_2}(h) = -\frac{V_z t_{sk}}{I_{xx}} h s_3 + q_{b_1}(\pi/2) + q_{b_2}(h), \quad 0 \leq s_3 \leq 0.6c \tag{16}$$

Region 4

Similarly to region 2, the integration in region 4 can be performed as a function of z, with $ds_2 = dz$.

$$q_{b_4}(z) = -\frac{V_z t_{sp}}{I_{xx}} \int_0^z z \cdot dz = -\frac{V_z t_{sp}}{2I_{xx}} z^2, \quad 0 \leq z \leq h \tag{17}$$

Region 5

Making use of the geometrical properties of similar triangles, the z coordinate can be expressed as a function of s_5, relation given as following $z = h - \frac{h}{l_{sk}} s_3$

$$q_{b_5}(s_5) = -\frac{V_z t_{sk}}{I_{xx}} \cdot \int_0^{s_5} (h - \frac{h}{l_{sk}} s_5) \cdot ds_5 + q_{b_3}(0.6c) + q_{b_4}(h) \tag{18}$$

$$q_{b_5}(s_5) = -\frac{V_z t_{sk}}{I_{xx}} (h s_5 - \frac{h}{2l_{sk}} s_5^2) + q_{b_3}(0.6c) + q_{b_4}(h), \quad 0 \leq s_5 \leq l_{sk}$$

Region 6

The z coordinate can be expressed with respect to s_6 as z=$-\frac{h}{l_{sk}} s_6$ using the properties for similar triangles.

$$q_{b_6}(s_6) = -\frac{V_z t_{sk}}{I_{xx}} \int_0^{s_6} -\frac{h}{l_{sk}} s_6 \cdot ds_6 + q_5(l_{sk}) = \frac{V_z t_{sk}}{I_{xx}} \frac{h}{2l_{sk}} s_6^2 + q_5(l_{sk}), \quad 0 \leq s_6 \leq l_{sk} \tag{19}$$

Region 7

The integration in region 7 can be performed as a function of z, with $ds_7 = dz$.

$$q_{b_7}(z) = -\frac{V_z t_{sp}}{I_{xx}} \int_0^z z \cdot dz = -\frac{V_z t_{sp}}{2I_{xx}} z^2, \quad -h \leq z \leq 0 \tag{20}$$

Region 8

Region 8 has a similar implementation as region 3.

$$q_{b_8}(s_8) = -\frac{V_z t_{sp}}{I_{xx}} \int_0^{s8} h \cdot ds_8 + q_{b_6}(l_{sk}) - q_{b_7}(-h) = -h \frac{V_z t_{sp}}{I_{xx}} s_8 + q_{b_6}(l_{sk}) - q_{b_7}(-h), \quad 0 \leq s_8 \leq 0.6c \tag{21}$$

Region 9

The integration in region 9 can be performed as a function of z, with $ds_9 = dz$.

$$q_{b_9}(z) = -\frac{V_z t_{sp}}{I_{xx}} \int_0^z z \cdot dz = -\frac{V_z t_{sp}}{2I_{xx}} z^2, \quad -h \leq z \leq 0 \tag{22}$$

Region 10

In region 10 the same approach as in region 1 is applied.

$$q_{b_{10}}(\theta) = -\frac{V_z t_{sk}}{I_{xx}} \int_{-\pi/2}^{\theta} h^2 sin\theta \cdot d\theta + q_{b_8}(0.6c) - q_{b_9}(-h) = -\frac{V_z t_{sk}}{I_{xx}} h^2 (cos\theta - 1) + q_{b_8}(0.6c) - q_{b_9}(-h), \quad -\pi/2 \leq \theta \leq 0 \tag{23}$$

The redundant shear flow can be found by setting the rate of twist to 0 as in Equation 24, which is applied in each cell, in order to provide a consistent twist of the entire cross-section (one cell can not have a different twist from the other cell).

$$0 = \oint \frac{q}{t} ds \tag{24}$$

The numerical values of the redundant shear flow can be found by solving the system given by Equation 25, which describes the shear flow in each of the three cells.

$$\begin{bmatrix} A_{11} & A_{12} & A_{13} \\ A_{21} & A_{22} & A_{23} \\ A_{31} & A_{32} & A_{33} \end{bmatrix} \begin{bmatrix} q_{0,1} \\ q_{0,2} \\ q_{0,3} \end{bmatrix} = - \begin{bmatrix} b_1 \\ b_2 \\ b_3 \end{bmatrix} \tag{25}$$

The components of the first matrix are given from Equation 26 to Equation 34 and represent the geometry integral $\oint \frac{ds}{t}$. The index indicates the geometry. For instance, the index 11 shows the geometry integral corresponding to the shear present in cell 1 only, whereas index 12 corresponds to the region that is exposed to the shear flow in both cell 1 and cell 2 (thus the spar web).

$$A_{11} = \int_0^{\pi/2} \frac{h}{t_{sk}} d\theta + \int_0^h \frac{ds}{t_{sp}} + \int_0^h \frac{ds}{t_{sp}} + \int_{-\pi/2}^0 \frac{h}{t_{sk}} d\theta \tag{26}$$

$$A_{12} = -\int_0^h \frac{ds}{t_{sp}} - \int_0^h \frac{ds}{t_{sp}} \tag{27}$$

$$A_{13} = 0 \tag{28}$$

$$A_{21} = -\int_0^h \frac{ds}{t_{sp}} - \int_0^h \frac{ds}{t_{sp}} \tag{29}$$

$$A_{22} = \int_0^{0.6c} \frac{ds}{t_{sk}} + \int_0^{0.6c} \frac{ds}{t_{sk}} + \int_0^h \frac{ds}{t_{sp}} + \int_0^h \frac{ds}{t_{sp}} - \int_0^h \frac{ds}{t_{sp}} - \int_0^h \frac{ds}{t_{sp}} \tag{30}$$

$$A_{23} = -\int_0^h \frac{ds}{t_{sp}} - \int_0^h \frac{ds}{t_{sp}} \tag{31}$$

$$A_{31} = 0 \tag{32}$$

$$A_{32} = -\int_0^h \frac{ds}{t_{sp}} - \int_0^h \frac{ds}{t_{sp}} \tag{33}$$

$$A_{33} = \int_0^{l_{sk}} \frac{ds}{t_{sk}} + \int_0^{l_{sk}} \frac{ds}{t_{sk}} + \int_0^h \frac{ds}{t_{sp}} + \int_0^h \frac{ds}{t_{sp}} \tag{34}$$

The total base shear flows in each cell are provided below in Equation 35, Equation 36 and Equation 37.

$$b_1 = \int_0^{\pi/2} \frac{q_{b_1} h d\theta}{t_{sk}} + \int_0^h \frac{q_{b_2}(y) dy}{t_{sp}} - \int_{-h}^0 \frac{q_{b_9}(y) dy}{t_{sp}} + \int_{-\pi/2}^0 \frac{q_{b_{10}} h d\theta}{t_{sk}} \tag{35}$$

$$b_2 = \int_0^h \frac{q_{b_2}(y)dy}{t_{sp}} + \int_0^{0.6c} \frac{q_{b_3}(s_3)ds_3}{t_{sk}} - \int_{-h}^0 \frac{q_{b_7}(y)dy}{t_{sp}} + \int_0^h \frac{q_{b_4}(y)dy}{t_{sp}} + \int_0^{0.6c} \frac{q_{b_8}(s_8)ds_8}{t_{sk}} - \int_{-h}^0 \frac{q_{b_9}(y)dy}{t_{sp}} \quad (36)$$

$$b_3 = \int_0^{l_{sk}} \frac{q_{b_5}(s_5)ds_5}{t_{sk}} + \int_0^{l_{sk}} \frac{q_{b_6}(s_6)ds_6}{t_{sk}} + \int_0^h \frac{q_{b_4}(y)dy}{t_{sp}} - \int_{-h}^0 \frac{q_{b_9}(y)dy}{t_{sp}} \quad (37)$$

Once the base and redundant shear flow are superimposed, the maximum shear flow in the cross-section can be identified.

4 Compression Load due to Bending

From the shear force distribution, the bending moment can be determined through Macaulay step functions. The point loads (the weight of the engines and the weight of the ribs) contribute to the bending moment when the value of the square brackets is positive. In this case, the y cursor starts from the tip to the root, in order to avoid the computation of reaction forces. The bending moment calculation is expressed in Equation 38 and its distribution is illustrated in Figure 4.

$$M_x(y) = \int_0^y V(y)dy + \sum W_{rib,i} \cdot [y - y_{rib}] + \sum W_{eng,i} \cdot [y - y_{eng,i}] \quad (38)$$

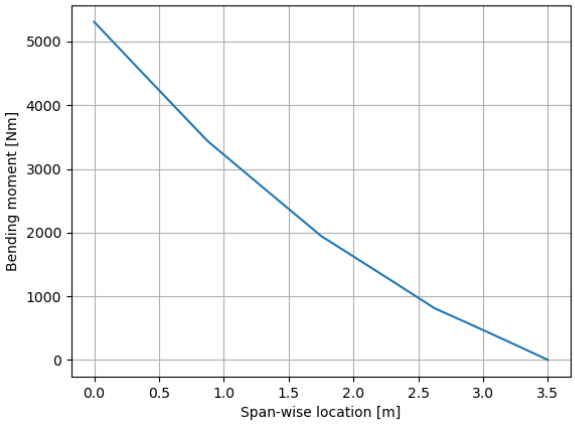

Figure 4: Bending Moment Distribution

The bending stress in a symmetric structure can be simply expressed by Equation 39 and the corresponding distributed compression load in Equation 40, where the total moment of inertia is computed in Equation 41 (accounting for stringers, wing-box skin and spars).

$$\sigma_x = \frac{M_x y}{I_{xx}} \quad (39) \qquad N_x = \frac{M_x z}{I_{xx} c(y)} \quad (40)$$

$$I_{xx} = n r_{st} I_{st} + A_{st}(0.5 \cdot H(y))^2 + \frac{t_{sp} H^3(y)}{12} + 2 \cdot 0.6 \cdot c(y) \cdot t_{sk}(0.5 \cdot H(y))^2 \quad (41)$$

Given the means to assess the stress level in wing box, constraints regarding structural instability and yielding during cruise, and failure for maximum load level can be set.

5 Constraints

The first six constraint are set for cruise condition, when the loading factor is 1. The last two conditions are set for the maximum loading factor, 2.5. In the process of structural design, usually it is desired to be able to predict and design for a certain failure mode. In the current case, during cruise, no instability is allowed and it is desired for the local skin buckling (due to combined contribution of shear and compression) to occur before any other structural instability, given that in general the buckling of the stringer leads to major loss in load carrying capacity, and global buckling could affect the stringer attachment to the skin. Thus, all of the other buckling critical loads should be higher than the critical load for local skin buckling due compression (the stringers only carry compression).

5.1 Combined Compression and Shear Load Buckling

The skin between the stiffeners can buckle when loaded in compression and/or shear, and this type of buckling is called local skin buckling. The critical buckling stress due to compression is given in Equation 42 and the corresponding compression force (in N/m)critical is expressed in Equation 43, where k is the buckling coefficient, depended on the boundary conditions and skin strip size. Figure 5 depicts the values of k for different boundary conditions and skin aspect ratios. It is considered that the stringers provide simply supported boundaries (corresponding to curve C in the plot), the buckling coefficient being 4, valid and conservative for any panel aspect ratio.

$$\sigma_{cr} = k\frac{\pi^2 E}{12(1-\nu)}\left(\frac{t_{sk}}{b_3}\right)^2 \qquad (42) \qquad\qquad N_{x,cr} = k\frac{\pi^2 E}{12(1-\nu)}\frac{t_{sk}^3}{b_3^2} \qquad (43)$$

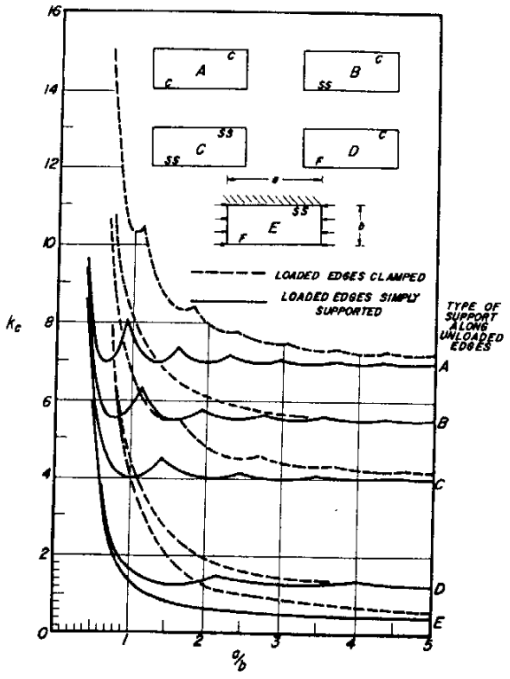

Figure 5: Compression Buckling Coefficient [2]

In a similar manner to the compression critical loads, the shear critical buckling stress is expressed by Equation 44 and the critical shear flow (in N/m) is given in Equation 45, but the buckling coefficient takes a different value, 5.35, as depicted in Figure 6.

$$\tau_{cr} = k_s\frac{\pi^2 E}{12(1-\nu)}\left(\frac{t_{sk}}{b_{st}}\right)^2 \qquad (44) \qquad\qquad N_{xy,cr} = k_s\frac{\pi^2 E}{12(1-\nu)}\frac{t_{sk}^3}{b_{st}^2} \qquad (45)$$

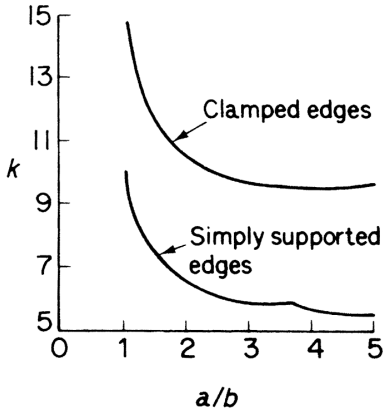

Figure 6: Shear buckling coefficient [4]

The combined effect towards buckling of both compression and shear can be quantified through Equation 46, stating the condition for which buckling does not occur in terms of distributed loads (N/m). This equation also represents the first constraint in the optimisation.

$$\frac{N_x}{N_{cr,x}} + \left(\frac{N_{xy}}{N_{cr,xy}}\right)^2 \leq 1 \longleftrightarrow \frac{N_x}{N_{cr,x}} + \left(\frac{N_{xy}}{N_{cr,xy}}\right)^2 - 1 \leq 0 \tag{46}$$

5.2 Local Skin Buckling<Global Skin Buckling

A stiffened panel can also buckle as a whole, Equation 42 being valid for global skin buckling calculations as well. In this case, the width of the panel is utilised instead of the stringer pitch, and simply supported conditions can be assumed. The contribution of the stringers that still provide a stiffening effect can be considered by smearing their thickness to the skin thickness, as in Equation 47.

$$t_{smeared} = \frac{t_{sk}b + nr_{st}t_{st}(h_{st} - t_{sk})}{b} \tag{47}$$

The smeared thickness is substituted in Equation 42 and the constraint is expressed in Equation 48.

$$\sigma_{cr,loc} \leq \sigma_{cr,glob} \longleftrightarrow \sigma_{cr,loc} - \sigma_{cr,glob} \leq 0 \tag{48}$$

5.3 Local Skin Buckling<Column Stringer Buckling

For simply supported stringers, the critical column buckling load of one stringer (in N) is given by Equation 49. In order to be able to compare it to the skin buckling load, the critical distributed compressive load acting on all stringers is computed in Equation 50, this approach being also conservative, given that in reality the skin beneath the stringer takes part of the compression load. The constraint is expressed in Equation 51.

$$P_{crit} = \frac{\pi^2 EI}{L^2} \tag{49}$$

$$N_{col} = \frac{P_{crit}}{2w_{st}} \tag{50}$$

$$N_{x,cr} \leq N_{col} \longleftrightarrow N_{x,cr} - N_{col} \leq 0 \tag{51}$$

5.4 Local Skin Buckling< Stringer Flange Buckling

The individual flanges of the stringer can also buckle, Equation 42 for skin buckling bring valid for their assessment. The buckling coefficient changes as one edge is free and one is simply supported, thus k is conservatively chosen to be 2. The constraint is expressed in Equation 52.

$$\sigma_{cr,loc} \leq \sigma_{cr,flange} \longleftrightarrow \sigma_{cr,loc} - \sigma_{cr,flange} \leq 0 \tag{52}$$

5.5 Local Skin Buckling< Stringer Web Buckling

Similarly to the flanges, the web of the stringer can also buckle and the critical load is computed with Equation 42 as well. The edges can be conservatively considered simply supported, the buckling coefficient k being 4. The constraint is expressed in Equation 53.

$$\sigma_{cr,loc} \leq \sigma_{cr,web} \longleftrightarrow \sigma_{cr,loc} - \sigma_{cr,web} \leq 0 \tag{53}$$

5.6 von Mises Yield Criterion

Plastic deformations are not allowed to occur during cruise flight, and in order to assess the stress level in the structure against yielding the von Mises yield criterion is used. The von Mises stress is expressed in Equation 54 and the constraint is stated in Equation 55.

$$\sigma_{VM} = \sqrt{\frac{1}{2}[(\sigma_{xx} - \sigma_{yy})^2 + (\sigma_{yy} - \sigma_{zz})^2 + (\sigma_{zz} - \sigma_{xx})^2] + 3(\tau_{xy}^2 + \tau_{yz}^2 + \tau_{xz}^2)} \tag{54}$$

$$\sigma_{VM} = \sqrt{\frac{1}{2}\sigma_{zz}^2 + 3\tau_{xz}^2}$$

$$\sigma_{VM} < \sigma_{yield} \longleftrightarrow \sigma_{VM} - \sigma_{yield} < 0 \tag{55}$$

5.7 Crippling

Crippling is a form of local buckling that occurs in columns, leading to the failure of the structure. It is related to plastic deformation of the stinger, and it is desired to have the load higher than the column buckling of the stringers (and subsequently higher than the local skin buckling), as crippling leads to the entire failure of the structure. The crippling load is expressed in Equation 56 (in N/m), where for aluminium alloys the constants are β=1.42, m=0.85, and for Z stringers g=5 [4]. The constraint is stated in Equation 57.

$$\bar{N_f} = t_{st}\beta\sigma_y\left[\frac{gt_{st}^2}{A_{st}}\sqrt{\frac{E}{\sigma_y}}\right]^m \tag{56}$$

$$N_{col} \leq \bar{N_f} \longleftrightarrow N_{col} - \bar{N_f} \leq 0 \tag{57}$$

5.8 Post Buckling

Once the stiffened panel buckles, it can still carry loads, but the load is re-directed to edges, where the level of the load is higher than the applied load. This can be seen as if only part of the skin is effective, not the entire width. The effective width (which only accounts for half of the plate!) is given in Equation 58 [3] for an isotropic material, as a function of the span-wise location and post buckling ratio.

$$b_{eff} = \frac{c(y)}{2 + 1.3\left(1 - \frac{P_{cr}}{P_x}\right)} \tag{58}$$

The total load experienced in post-buckling is expressed in Equation 59, where N_x is the distributed force within the structure, thus the actual load level (given that the load is assumed to be distributed uniformly on the entire width).

$$P_x = 2N_x b_{eff} \tag{59}$$

$$F_{uts} = \sigma_{uts} \cdot A = \sigma_{uts} \cdot (nr_{st}A_{st} + 0.6 \cdot c(y)) \tag{60}$$

As the panel should hold loads until failure for a load factor of 2.5, the aerodynamic loading is multiplied with 2.5 and the post-buckling ratio (load level divided by critical buckling load) for which the current design is created is 2.5. The maximum load experienced within the plate can not be higher than the ultimate load, which leads to the constraint in Equation 61.

$$P_x \leq \frac{100}{139} F_{uts} \longleftrightarrow P_x - 0.72F_{uts} \leq 0 \tag{61}$$

6 Formal expression of the optimisation

The formal expression of the optimization problem is provided below. Because the Python optimiser sets by default the constraints to be greater or equal to 0, the mathematical formulations of the constraints below correspond to the code implementation.

$$f_{\mathbf{min}} = W_{wing} \tag{62a}$$

$$\begin{aligned}
\text{subjected to} \quad & 1 - \frac{N_x}{N_{cr,x}} + \left(\frac{N_{xy}}{N_{cr,xy}}\right)^2 \geq 0 && c_1 && \text{(62b)}\\
& \sigma_{cr,glob} - \sigma_{cr,loc} \geq 0 && c_2 && \text{(62c)}\\
& \sigma_{cr,flange} - \sigma_{cr,loc} \geq 0 && c_3 && \text{(62d)}\\
& \sigma_{cr,web} - \sigma_{cr,loc} \geq 0 && c_4 && \text{(62e)}\\
& N_{x,cr} - P_{cr} \geq 0 && c_5 && \text{(62f)}\\
& \sigma_{yield} - \sigma_{vms} \geq 0 && c_6 && \text{(62g)}\\
& \bar{N_f} - N_{col} \geq 0 && c_7 && \text{(62h)}\\
& 0.72F_{uts} - P_x \geq 0 && c_8 && \text{(62i)}
\end{aligned}$$

$$X = [b, c_r, t_{sp}, t_{rib}, L, b_{st}, h_{st}, t_{st}, w_{st}, t] \qquad \text{design vector} \tag{62j}$$

References

[1] J. Alba-Maestre et al. "Final Report - Multi-Disciplinary Design and Optimisation of a Long-Range eVTOL Aircraft". In: (Nov. 2021). DOI: 10.5281/zenodo.5741614.

[2] E. F. Bruhn. *Analysis and Design of Flight Vehicle Structures*. Jacobs Pub, 1973. ISBN: 10 0961523409.

[3] C. Kassapoglou. *Design and analysis of composite structures: With applications to aerospace structures, 2nd ed.* New York: John Wiley & Sons, 2013. ISBN: 9780470972632.

[4] T.H.G.Megson. *Aerospace Structural Design an Analysis, 4th ed.* Oxford, UK: Elsevier, 2007. ISBN: -13: 978-0-75066-7395.